Mechanism and Characteristics of High-Frequency Pulsed Jet Circulation Control

IOP Conf. Series: Materials Science and Engineering **608** (2019) 012021 doi:10.1088/1757-899X/608/1/012021

Mechanism and Characteristics of High-Frequency Pulsed Jet Circulation Control

Ren Zhan, Deng-cheng Zhang, Yan-hua Zhang, Wu-ji Zheng and Yi-wen Li

Aeronautic Engineering Technology College, Airforce Engineering University, 710038 Xi'an, China

Corresponding author: Dengcheng Zhang@dengcheng_zhang@sina.com

Abstract: Conventional circulation control technology presents problems in certain situations. Pulsed jet circulation control appears to be a feasible alternative to solve such problems, especially for the high-frequency pulsed jet (HFPJ). To acquire the aerodynamic characteristics of the HFPJ and reveal the mechanism behind it, numerical simulation is conducted using a verified computational fluid dynamics（CFD）method. The action mode of the pulsed jet characterized by equilibrium and oscillation is proposed according to the analysis of a dynamic procedure. Lift and drag characteristics are obtained, defining the critical frequency to demarcate high and low frequencies. An oscillation function is also established to illustrate the difference between the characteristics of the HFPJ and a low-frequency pulsed jet (LFPJ) by analyzing the simulation results. The pressure distribution and flow field in the simulation results explain the stall characteristic of the HFPJ. Series results indicate the HFPJ demonstrates superior lift augmentation and drag reduction compared to the LFPJ and steady jets.

1 Introduction

Circulation control technology based on the Coanda effect[1] has been widely studied since the 1930s. Circulation control airfoil (CCA) [2] consists of conventional airfoil and a circular trailing edge [3]. First, a plenum is opened in the wing interior while a small slot is established on the trailing edge of the upper wing. The jet sheet (i.e., wall jet) is ejected from the slot through the inner tube tangent to the trailing edge. The jet sheet mixed with the external flow circles the trailing edge under the action of pressure and centrifugal force with delayed boundary layer separation. The effect produces substantial lift augmentation in the airfoil, with the greatest incremental lift efficiency ($\Delta C_l/\Delta C_u$) exceeding 80 and reducing the landing speed of the plane by approximately 50%[4]. Relevant research has been carried out by Englar and others. The medium height slot, low momentum coefficient, and small angle of attack (AOA) are conducive to lift augmentation[1][5][6]. The United States Navy utilized the A-6A CCW/ short take-off and landing (STOL) aircraft to conduct flight tests to verify STOL on circulation control technology [7][8]. In addition, series tests were developed by colleges and universities including West Virginia University[9–12].

Circulation control technology offers advantages in lift augmentation and noise reduction but also has inherent disadvantages: the sharp increment of induced drag increases the drag coefficient as the AOA grows, potentially leading to an abrupt stall on the wing[13]. A higher mass flow rate of the steady jet originating from the engine increases corresponding drag[14][15]. The emergence of circulation control technology in the pulsed jet alleviates some adverse effects of conventional jets. Meanwhile, pulse-jet circulation control achieves a similar or identical lift augmentation effect with a smaller mass flow rate[16]. Although

experimental and numerical studies have been carried out by Oyler and Schatz et al[17][18], study conditions were limited to low frequency, low Mach number (0.1Ma), and an AOA equal to 0. Drastic fluctuation in aerodynamic characteristics occurs under these conditions; thus, the advantages of the pulsed jet cannot be fully realized. Compared with no blowing circulation control technology, the lift characteristics are greatly improved by using a steady jet or low-frequency pulsed jet (LFPJ), although better drag characteristics are hard to achieve simultaneously. The high-frequency pulsed jet (HFPJ) has therefore been studied systematically as the basis for predecessors to eliminate defects.

In this paper, the critical frequency for distinguishing the HFPJ and LFPJ is presented according to the frequency characteristics of the pulsed jet. Preliminary research on the characteristics and mechanism of the HFPJ has been conducted. Results show that drag characteristics are greatly improved, an advantage that is otherwise unattainable in a traditional high-lift system or circulation control using a steady jet. The conclusions provide theoretical evidence for continued research on aircraft performance when applying the circulation control technique using the HFPJ.

2 Introduction of Numerical Simulation Method

The following case was simulated using ANSYS CFX. The main control equation is an unsteady compressible Reynolds average N-S equation. SST[19] was utilized as the turbulence model, and the finite element method (FEM) was adopted to discretize the equation. The time step was set at 0.01T(period of the jet sheet). Mach number of the flow was set to 0.1 with the total pressure 1 atm. The supercritical airfoil indicated in Fig. 1 was adopted to generate the applied CCA as the baseline.

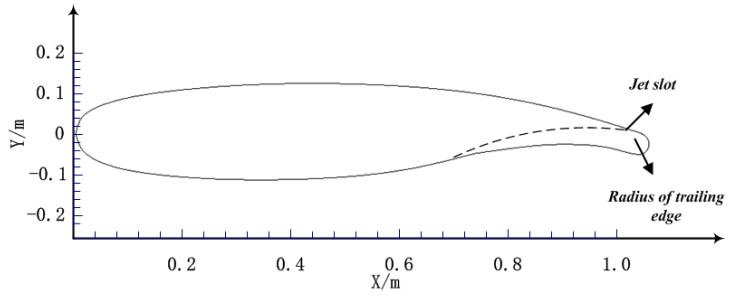

Figure 1. The applied CCA.

The impulse function of $v_{jet}(t)$ is defined as follows:

$$v_{\text{jet}}(t)=\begin{cases}2v_{jet-av}\cdots\cdots\left(t\in\left(\dfrac{k}{f},(2k+1)\dfrac{1}{2f}\right)\right)\\ 0\cdots\cdots\left(t\in\left((2k+1)\dfrac{1}{2f},(k+1)\dfrac{1}{f}\right)\right)\end{cases} \tag{1}$$

where v_{jet-av} is average jet velocity. $c_{\mu-av}$ is defined similarly to v_{jet-av}.

To accurately simulate the complicated pulse flow field around the Coanda surface, the proposed method are as follows: considering the complicated flow field near the slot, airfoil rear (under a large AOA), leading edge, and trailing edge, the mesh of those areas is densified to confirm the precision of the calculation distinguished by different methods of increasing nodes at the edges. The height of the first layer grid was set to 1.0×10^{-6} m such that $y^{+}<1$.The model included 339410 cells as shown in Fig.2. Different structural grid scales (G1–4) were adopted to verify grid independence with 210860, 276740, 324972, and 411800 cells, respectively.

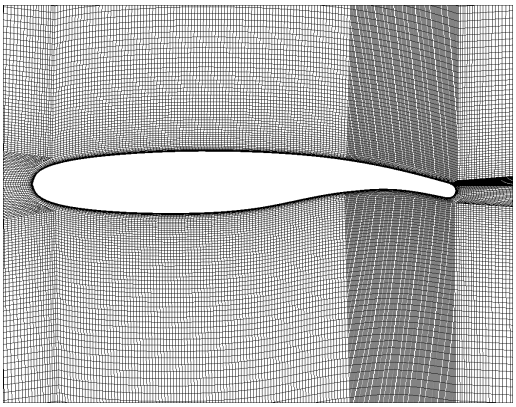

Figure 2. Adopted computational grid with 339410 cells.

The CCA from the reference[20] was used to verify the calculation method. The calculated results were consistent with experimental data from the reference[20], depicted in Fig. 3 for G1–4, indicating that the CFD calculation method is appropriate for numerical simulation of the HFPJ in the subsequent chapters. The time step was set at 0.05*T* for each cycle.

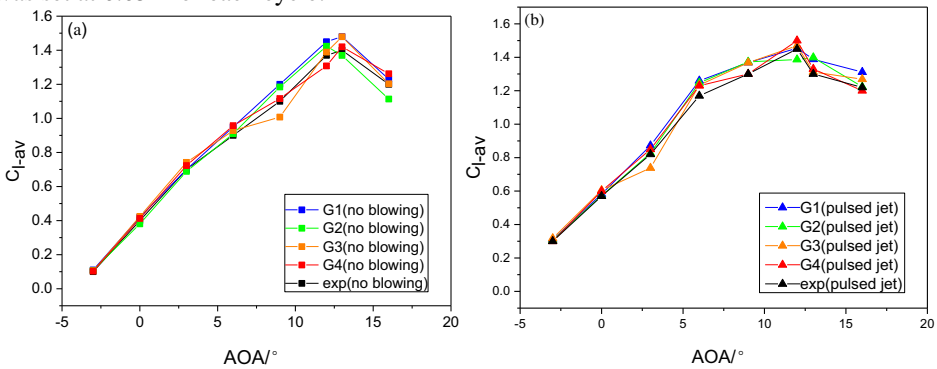

Figure 3. Validation of CFD method: (a)no blowing; (b) pulsed jet

3 Results and Discussion

3.1 Action Mode of Pulsed Jet Circulation Control

The composition of the pulsed jet is twofold, containing jet-effective and jet-ineffective parts for any frequency of the pulsed jet *f*. The function is the acquisition of equilibrium and periodic variation of circulation caused by periodic changes in the flow field. The mechanism of the HFPJ circulation control is illustrated in Chapter 3;and the flow field around the trailing edge of the airfoil at two frequencies (10Hz) is displayed in Fig. 4.

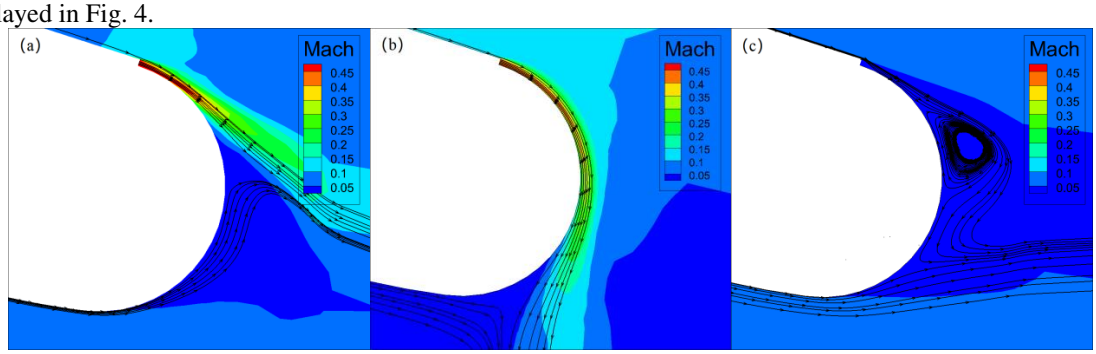

Figure 4. Flow field around the trailing edge at two different frequencies: (a) f = 10Hz ($t/T\rightarrow0$); (b) f = 10Hz (t/T =0.5); (c) f = 10Hz ($t/T\rightarrow1$)

In the simulation, before acquiring the equilibrium, the jet from the slot on the trailing edge began to function at t = 0. The consequent input momentum accelerated the boundary layer flow, deflecting the streamline encircling the Coanda surface. The delay in separation produced more circulation around the airfoil along with lift (C_l) and drag (C_d). Circulation around the airfoil peaked at t = 0.5T. The jet sheet disappeared when t > 0.5T, and the flow continued to move around the Coanda surface at a short distance due to inertia. The current separation point could not be maintained due to the high pressure drag with no input momentum. At the same time, separation was enhanced and upper flow started to decelerate along with a circulation destruction that reduced C_l. C_d declined as the static pressure increased and the flow decelerated, concluding the entire process cycle. The flow field was changed despite the jet being stopped (streamline deflection) compared to the initial condition (t = 0). As such, the increment of circulation was positive in a single cycle. If the jet sheet was re-imposed before the increment decreased to 0, circulation restarted with a micro-increment of circulation in every cycle before the equilibrium. Accumulation in a cycle changed to 0 under the equilibrium. After completion of the above process, periodic oscillation of the circulation occurred within a specific frequency in a certain range. This trend also held true for circulation, C_l, and C_d. Meanwhile, number of experienced cycles before the equilibrium n depends on the frequency of the pulsed jet, illustrated in Fig. 5.

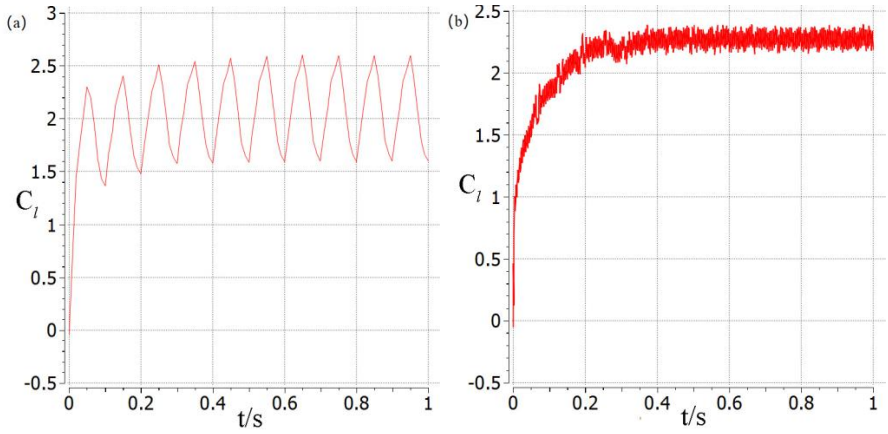

Figure 5. Procedure of reaching equilibrium: (a) f = 10Hz;(b) f = 200Hz.

The difference in aerodynamic characteristics between un-equilibrium and equilibrium indicated in Fig. 5 is related to the difference in the flow field around the rear lower surface of the CCA, except for the distinction of the upper-surface flow field as the main reason. A high-velocity region on the upper surface flow also expanded as time passed due to the gradually delayed boundary separation. Moreover lower surface flow decelerated in the process of approaching the equilibrium, a trend induced by the high-static-pressure area located on the lower part of the trailing edge that provides a high pressure gradient as shown in Fig.6. The high pressure gradient disappeared when equilibrium was achieved.

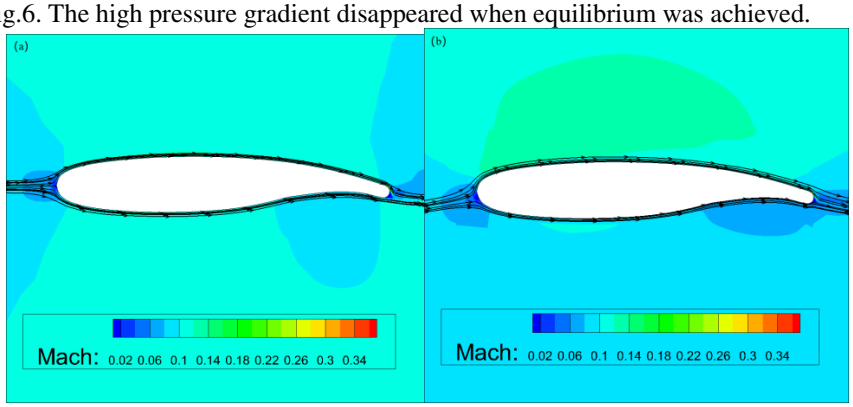

Figure 6. Flow field of CCA lower surface (200Hz, t/T = 0.5): (a) un-equilibrium;(b) equilibrium

3.2 Aerodynamic Characteristics and Mechanism of HFPJ Circulation Control

Lift and drag characteristics are profoundly affected by the frequency of the pulsed jet. Therefore, it is

necessary to study the frequency characteristic of the pulsed jet to identify the optimal frequency range. Fig. 7 shows the curve of lift and drag characteristics that shifted in line with the frequency at a certain $C_{\mu\text{-}av}$. Average lift coefficient $C_{l\text{-}av}$ and average drag coefficient $C_{d\text{-}\mathrm{av}}$ are defined as follows:

$$C_{l-av} = \frac{1}{T}\int_0^T C_l(t)dt \tag{2}$$

$$C_{d-\mathrm{av}} = \frac{1}{T}\int_0^T C_d(t)dt \tag{3}$$

Fig. 7(a) shows that average lift coefficient increment$\Delta C_{l\text{-}av}$ diminished first and grew later as the frequency increased. It tended to be equal to that of the steady jet and remained constant once the frequency exceeded 300Hz. Fig. 7(b) shows that $C_{d\text{-}\mathrm{av}}$ diminished to a specific value at a higher frequency and then stayed constant. Above all, the characteristic showed significant differences between the HFPJ and no blowing or LFPJ. The$\Delta C_{l\text{-}av}$ of the HFPJ appeared to remain constant when the frequency was above a specific value. The HFPJ is supposed to be characterized by this unique feature. Thus, in the demarcating method, the critical frequency of circulation control using the pulsed jet is defined as the point at which $C_{l\text{-}\mathrm{av}}$ remains constant, and the high/low frequency is higher/lower than that. The results indicate that the respective effects of lift augmentation and drag reduction were improved by using the HFPJ.

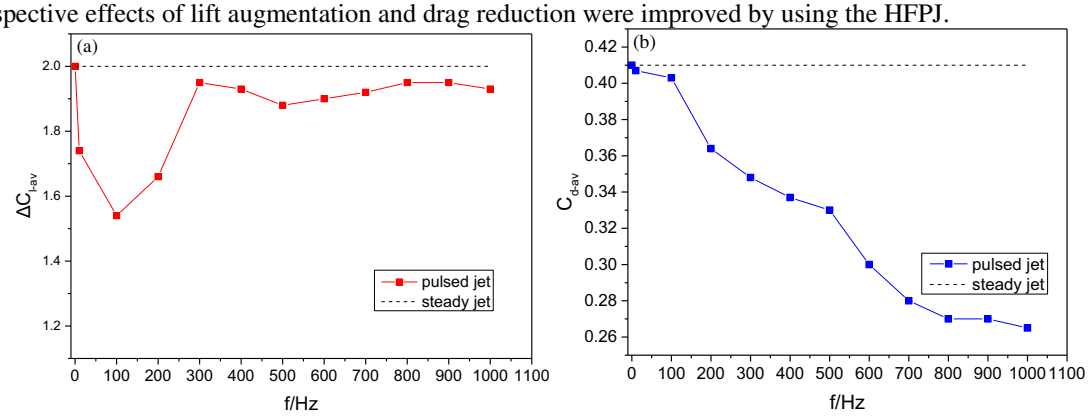

Figure 7. Frequency characteristic curve: (a) average incremental lift coefficient; (b) average drag coefficient

According to the action mode of the pulsed jet, circulation appeared to increase and decrease in two different parts. To reveal the mechanism of lift and drag characteristics of the HFPJ, a model of the accumulating circulation process from the initial state to the equilibrium was established. Moreover, an oscillation model was proposed to explain the rule of circulation at the equilibrium of C_l. Assume that a series of equilibria are distinguished by frequencies.

Periodic oscillating function of the circulation at equilibrium $\Gamma(t)$ is defined as follows:

$$\Gamma(t) = \Gamma_M + \mathrm{F}(t) \tag{4}$$

where F(t) is negative circulation function of the fluctuating value

The relationship between T_F and f is expressed as

$$T_F = \frac{1}{f} \tag{5}$$

where T_F is period of F(t)

According to the oscillation model, the different aerodynamic equilibrium states differentiate the time characteristics of circulation (ΔC_l). The distinction between peak of Γ_M and trough of Γ_m symbolizes the change in the equilibrium point at different frequencies. Γ_M and Γ_m collectively determine $\Delta C_{l\text{-}av}$ as

shown in Fig. 8. Γ_M dominates $\Delta C_{l\text{-}av}$ when $f < 200$Hz and nearly reaches a constant value above f = 300Hz, whereas Γ_m dominates $\Delta C_{l\text{-}av}$ when $f > 200$Hz. This conclusion is exemplified in Fig. 8, and the rule of Γ_M and Γ_m is as follows: under the influence of the combination of Γ_M and Γ_m, the $\Delta C_{l\text{-}av}$ might reach an extreme value as the frequency increases, as depicted in Fig. 8. Variation in $\Delta C_{l\text{-}av}$ depends on Γ_M and Γ_m in two respective situations ($f > 200$Hz and $f < 200$Hz).

The delay of separation, or the position of the separation point, represents the value of Γ_M. Conada turning angle, θ_{jet} (transient value; the variable changes over time) is recognized as the measurement of the displacement of the separation point along the Coanda surface. Given that the pressure gradient rises as θ_{jet} increases, it becomes harder for the jet sheet to overcome the larger gradient with a lower θ_{jet} increasing rate $\frac{d\theta_{jet}}{dt}$ until it declines to 0. This process facilitates circulation accumulation to focus on the time before $\frac{d\theta_{jet}}{dt}$ starts to decline sharply. In the simulation, θ_{jet-m} at different frequencies demonstrated negligible change based on frequency over 100Hz: maximum $\frac{d\theta_{jet}}{dt}$ (t/T = 0.5) of pulsed jet $\frac{d\theta_{jet-M}}{df}$ remained virtually constant if the corresponding jet-effective time was close to that mentioned above, such that Γ_M changed little at frequencies over 300Hz as well.

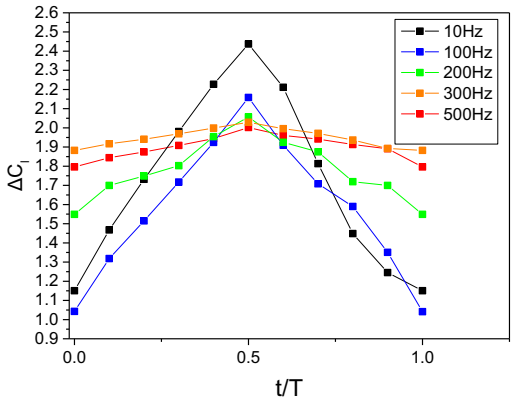

Figure 8. Time characteristics of lift coefficient increment.

The Γ_m achieved higher values at high frequencies according to Fig 8. As shown in Fig. 9, the boundary layer separation on the Coanda surface consisted of successive deceleration and detachment from to the flow. Deceleration, or moving backward from the separation point, occurred more quickly than detachment. This process operates as follows: after jet termination, the rest momentum of the jet transfers from the fluid region (closer to the slot) to the separation point. Thus, the position of the separation point can be maintained or changed slightly if the jet-ineffective time is sufficiently brief. On the other hand, centrifugal force declines as the flow decelerates, contributing to attachment on the Coanda surface of the flow. A regenerative jet sheet in the next cycle replenishes momentum to the boundary layer before the rest momentum in the current cycle can be counteracted by the impulse of the pressure gradient and frictional drag if the frequency is high enough. Consequently, boundary separation is better at high frequencies when $t/T \rightarrow 1$. This phenomenon explains whyΔC_l at f = 100Hz was much lower than that at f = 500Hz as shown in Fig. 9 (i.e., because deceleration started and continued for a period of time).

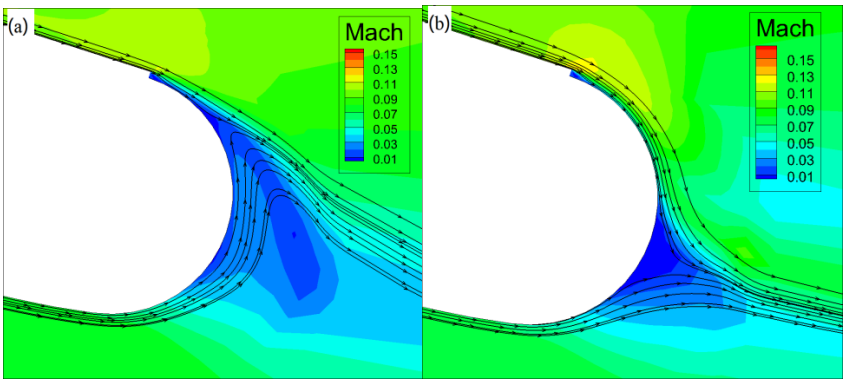

Figure 9. Flow field around the trailing edge at 10Hz and 500Hz ($t/T \rightarrow 1$): (a) f = 100Hz; (b) f = 500Hz

As for drag, the reduced jet-effective time resulted in displaced separation up along the Coanda surface as the frequency increased, leading to an increase in static pressure at the trailing edge and reducing the pressure drag.

In terms of the action mode of the pulsed jet, the corresponding shorter effective and ineffective time for the HFPJ resulted in relatively high Γ_m, along with Γ_M nearly equal to that of LFPJ. Higher $\Delta C_{l\text{-}av}$ is attributed to Γ_m and Γ_M at high frequencies. Compared to the LFPJ and steady jet, the HFPJ reduced drag via undermined pressure drag at the equilibrium. The distinction of the pressure distribution at the trailing edge between the HFPJ and LFPJ contributed to refined drag characteristics due to pressure drag reduction.

3.3 Stall Characteristics of High-frequency Pulsed Jet

Under conditions of different respective circulation controls, namely steady jet, the HFPJ at either 200Hz or 500Hz, and no blowing with $C_{\mu-av}$ = 0.02, the curve of changes in the lift-drag coefficient with AOA was obtained through numerical simulation; see Fig 11. The stall AOA (10°) under steady-jet circulation control was relatively low compared to under a no-blowing condition at small AOA. $C_{d\text{-}av}$ increased slowly and showed no sharp increase above 20°. The stall AOA (15°) under conditions of the HFPJ jet and no blowing was nearly equal: $C_{l\text{-}av}$ declined slowly and maintained a higher value as HFPJ was imposed when AOA exceeded the stall AOA. The drag characteristic was improved by HFPJ circulation control as shown in Fig. 10(b); that is, $C_{d\text{-}av}$ was less than AOA when applying HFPJ circulation control.

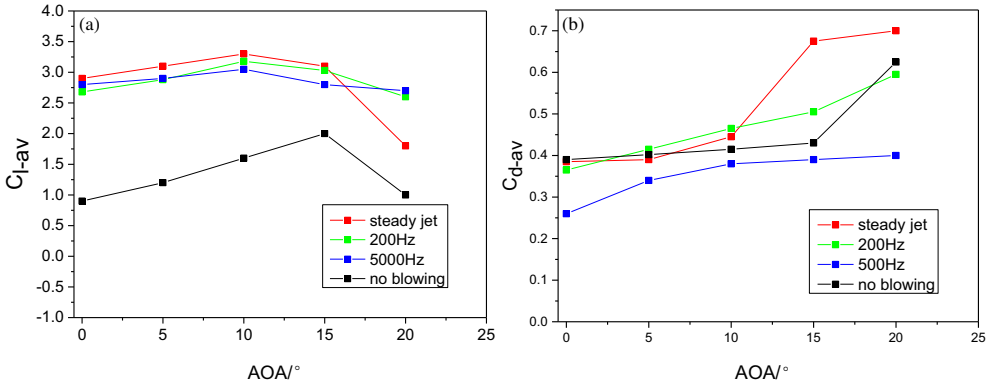

Figure 10. Lift-drag characteristic curve: (a) lift characteristic curve; (b) drag characteristic curve

With the flow field distribution of the steady jet and HFPJ at a certain time with no blowing, respectively, the time of the simulated flow field represents when the transient lift and average lift are equal. As shown in Fig. 11, stall became most serious when no jet circulation control was applied, but it was greatly alleviated by the HFPJ with deflection of streamlines leading to lower particular AOA and elimination of vortex.

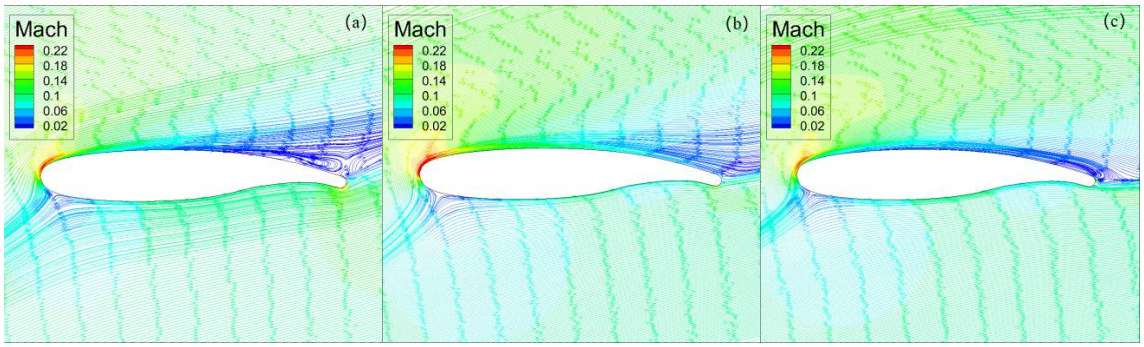

Figure 11. Flow around airfoil at 20° :(a) no blowing;(b) steady jet; (c) high-frequency pulsed jet

Fig. 12 illustrates the pressure diagrams of the trailing edge when AOA = 20° with different forms of circulation control. All conditions were set at the same reference pressure to determine a conclusion by comparison. The high-pressure region expanded clearly with the HFPJ compared to the steady jet and no blowing, leading to improved drag characteristic of the HFPJ as depicted in Fig. 11: the HFPJ increased the area of the high-pressure region around the rear of the airfoil and thus reduced pressure drag. In addition, frictional drag was nearly invariable because it was unaffected by variation in the small AOA; hence, the drag became lower overall as the HFPJ was imposed. The frictional drag affected the total drag chiefly by increasing the drag along with the AOA.

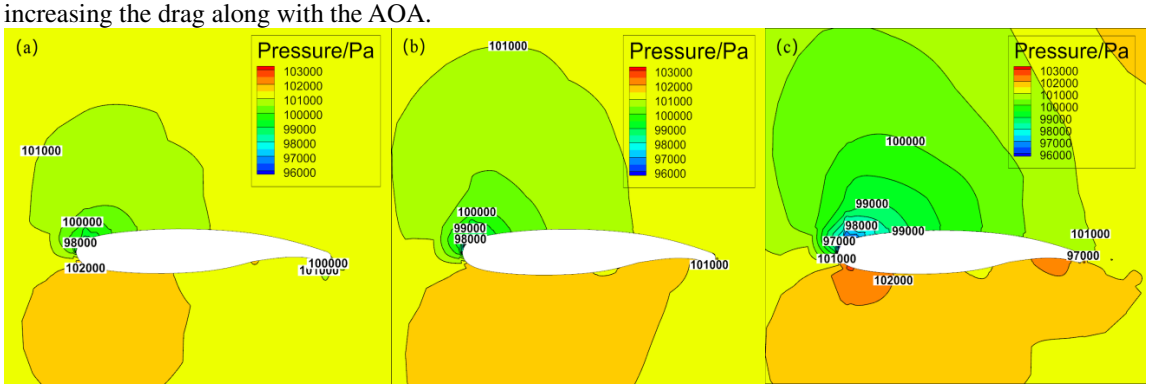

Figure 12. Pressure counter of airfoil at 20 ° : (a) no blowing; (b) steady jet; (c) high-frequency pulsed jet

4 Conclusion

In this study, the action mode of the pulsed jet is described in a procedure to reach and maintain the equilibrium of the circulation around the airfoil using the given mechanism. Lift characteristics of the pulsed jet identified the critical frequency (300Hz in the simulated case) to confirm the high or low-frequency range. The HFPJ circulation control exhibits particular advantages in lift augmentation and drag reduction by oscillation model: the HFPJ increases the maximum and minimum value of circulation in a cycle by modifying the boundary layer separation condition. Pressure drag is reduced by narrowing the region of low static pressure around the trailing edge. For the stall characteristic, the HFPJ expands the high-pressure region and reduces effective AOA, thereby increasing the stall AOA while reducing pressure drag. The simulation results must be verified by experiments but provide a reference for future studies.

References

[1] Englar RJ., and Huson G. Development of advanced circulation control wing high-lift airfoils. Journal of Aircraft 2012;21:476-483.

[2] Nielsen J. and Biggers J. Recent progress in circulation control aerodynamics. In: 25th AIAA Aerospace Sciences Meeting, Aerospace Sciences Meetings, Reno, USA, 24 March - 26 March 1987, AIAA 1987-1. Reston: AIAA.

[3] Zhu Z and Zongcheng W. Study of the circulation control technology. Acta Aeronautica Et Astronautica Sinica 2016; 37:411-428.

[4] Englar RJ and Williams RM. Test techniques for high-lift, two-dimensional airfoils with boundary layer and circulation control for application to rotary wing aircraft. Canadian Aeronautics and Space Journal 1975; 19:93-108.
[5] Zhang SY, Zhong YC, Peng-Zhe FU, et al. Numerical investigation of dual-radius in circulation control airfoil aircraft design. Aircraft Design 2011;31:1-6.
[6] Abramson J, Rogers E. High-speed characteristics of circulation control airfoils. In: 21st Aerospace Sciences Meeting, Reno, USA, 10 January - 13 January 1983 ,paper no. 83-0265. Reston: AIAA.
[7] Englar RJ, Hemmerly RA, Taylor DW, et al. Design of the circulation control wing STOL demonstrator aircraft. Journal of Aircraft 2015; 18:51-58.
[8] Pugliese A. and Englar R. Flight testing the circulation control wing. In: Aircraft Systems and Technology Meeting, Aircraft Design and Technology Meeting, New York, USA, 20 August - 22 August 1979, AIAA 1979-1971.Restion: AIAA.
[9] Broniatowski M. Circulation controlled STOL wing optimization. Journal of Aircraft 1984; 21:128-134.
[10] Sparks R, Michie S, and Crowther W. Development of an integrated circulation control Fluidic thrust vectoring flight test demonstrator. Texas Heart Institute Journal 2005; 32:194-197.
[11] Fielding J, Lawson C, Rui MP, et al. Design, build and flight of The DEMON demonstrator UAV. In: 11th AIAA Aviation Technology, Integration, and Operations (ATIO) Conference, Virginia Beach, USA, 20 September - 22 September 2011, AIAA 2011-6963. Reston: AIAA.
[12] Buonanno A, Cook MV, Erbsloeh SD. Flight Dynamic Simulation of a Flapless Flight Control UAV. In: 25th International Congress of the Aeronautical Sciences, 2006:1-11.
[13] Yaros SF, Sexstone MG, Huebner LD, et al. Synergistic airframe-propulsion interactions and integrations: a white paper prepared by the 1996-1997. Technical Report, Langley Aeronautics Technical Committee, USA, April 1998.
[14] Gregory J., Sally V., Anthony W, et al. An active flow circulation controlled flap concept for general aviation aircraft applications. In: 1st Flow Control Conference, Fluid Dynamics and Co-located Conferences, St. Louis, USA, 24 June - 26 June 2002, AIAA 2002-3157. Reston: AIAA.
[15] Kind RJ and Maull DJ. An experimental investigation of a low-Speed circulation-controlled aerofoil. Aeronautical Quarterly 1968; 19:170-182.
[16] Jones G and Englar R. Advances In Pneumatic Controlled High Lift Systems Through Pulsed Blowing. In: 21st AIAA Applied Aerodynamics Conference, Fluid Dynamics and Co-located Conferences, Orlando, USA, 23 June - 26 June 2003, AIAA 2003-3411.Reston: AIAA.
[17] Oyler TE and Palmer WE. Exploratory Investigation of Pulse Blowing for Boundary Layer Control.1st ed. 1972.
[18] Schatz M. and Thiele F. Numerical study of high-lift flow with separation control by periodic excitation. In: 39th Aerospace Sciences Meeting and Exhibit, Aerospace Sciences Meetings. Reno, USA, 08 January - 11 January 2001,AIAA 2001-296. Reston :AIAA.
[19] Rumsey CL and Nishino T. Numerical study comparing RANS and LES approaches on a circulation control airfoil. International Journal of Heat & Fluid Flow, 2011; 32:847-864.
[20] Shah N, Chi W, Kontis K. Active Flow Control Using Steady and Pulsed Blowing at Subsonic Speeds. In: 46th AIAA Aerospace Sciences Meeting and Exhibit, Reno, USA, 07 January - 10 January 2008,AIAA 2008-742.Reston:AIAA